ORIGINAL ARTICLE

Experimental and numerical study on SMA modified with an encapsulated polymeric healing agent

Sergey Inozemtcev · Denis Jelagin · Evgeniy Korolev · Hassan Fadil ·
Manfred N. Partl · Toan Do Trong

Abstract The present study aims at experimentally and numerically investigating the effect an encapsulated healing agent on the mechanical characteristics of a stone mastic asphalt (SMA). As a healing agent a thiol-containing urethane AR-polymer is used in this study. In order to gain a numerical insight into mechanical behavior of the capsules in SMA, a micromechanical finite element modeling is employed. The developed model allows capturing the stresses induced in the capsules at different load cases applied to the SMA on macro-scale. Particular attention is paid presently to the numerical evaluation of the local stress state that arises around capsules during compaction, operation, and also during crack initiation. SMA mixtures with various volumetric contents of healing capsules were manufactured and the capsules survival during mixture production was evaluated based on X-Ray Computed Tomography measurements. The effect of capsules on the self-healing properties of asphalt mixtures has furthermore been examined with repeated compressive strength tests. The obtained experimental results indicate that the absolute majority of capsules survive mixture production, and that their addition increases the SMA strength recovery during the healing period. The experimental and numerical results concerning capsules breakage are found to be in reasonable agreement. The developed micromechanical model may thus potentially provide a useful tool for optimization of capsules mechanical properties in order to improve their survival during mixture production as well as their timely activation.

Keywords Self-healing · Asphalt concrete · Capsule · Healing agent · FEM · Micromechanics

S. Inozemtcev · T. Do Trong
Department of Building Materials Science, National Research Moscow State University of Civil Engineering, Moscow, Russia

D. Jelagin (✉) · H. Fadil · M. N. Partl
Department of Civil and Architectural Engineering, KTH – Royal Institute of Technology, Stockholm, Sweden
e-mail: denis.jelagin@abe.kth.se

E. Korolev
Research and Education Center (Nanomaterials and Nanotechnology), National Research Moscow State University of Civil Engineering, Moscow, Russia

1 Introduction

Cracking through fatigue, static overloading or freezing is one of most common distress modes for asphalt pavements, which requires costly maintenance and repair. It starts with micro-cracks formation in asphalt's binder phase or at the stone-binder interface, which later coalesce and form macro-cracks. At the same time, micro-cracks in asphalt mixtures may gradually close during the load free periods due to viscoelastic flow of the binder phase in warm seasons,

thus preventing formation of macro-cracks. This self-healing behavior of asphalt mixtures may extend the service life of asphalt pavements with respect to crack formation. However, this effect should not be over-rated, because, in order to avoid high temperature rutting, pavements are generally designed stiff enough to carry high traffic loads at summer temperatures without significant permanent deformations [1].

Recently, a number of bituminous material designs have been proposed aiming at improving healing capabilities of those materials, cf. e.g. [2]. One promising way to enhance the self-healing potential of asphalt mixtures is the use of encapsulated binder-modifiers, which are activated after the destruction of the capsules during the formation of cracks [3–8]. In particular, as shown in [4, 5] average healing levels achieved for asphalt mixture samples with encapsulated sunflower oil is 40…50% of the initial strength. At the same time, there are certain challenges associated with use of encapsulated modifiers in asphalt mixtures. In order to survive the mixture production and compaction, the capsules containing a modifier must have sufficient thermal stability [9–11] and strength. The collapse of capsules during mixture production, will result in premature release of the modifier, which may lead to aggregate segregation and decrease in its shear stability. At the same time, the capsules should be sufficiently weak and brittle, to break due to stress concentration when micro-cracks are formed in their vicinity.

In view of these complex requirements, fabrication and design of capsules and their use for asphalt concrete for different applications has drawn a lot of attention recently [1, 12, 13]. Recently, [14, 15] the possibility of controlling the release of healing agent through microwave and induction heating has been evaluated. In order to avoid a one-shot self-healing effect, ideally, the capsules within the asphalt mixture should also be of different mechanical resistance. This would lead to gradual breaking of the capsules over the whole in-service period of the pavement and therefore foster a long-term self-healing effect. However, in that respect, research is only at the very beginning. This study may be considered as one contribution towards this goal.

The physical, geometrical and mechanical properties of capsules, may be controlled through chemical formulation and technological properties of suspensions used to encapsulate the modifiers. In particular,

as shown in [16–18], for the capsules where rejuvenating agent (RA) is encapsulated in a calcium alginate shell, the capsules diameters and wall thicknesses are effectively controlled through adjusting the alginate/rejuvenator ratio. Accordingly, capsules with different sizes and mechanical properties may be obtained in a straightforward manner. In order to optimize the properties of the capsules, ensuring their timely activation, a thorough understanding of stress distributions arising in the capsules vicinity during asphalt mixture production and its service life is necessary.

In literature a considerable number of recent studies exists, focusing on various aspects of self-healing asphalt mixtures, cf. e.g. [19–21]. The absolute majority of those studies are focused, however, on the development of the self-healing technology and experimental assessment of the effectiveness of the proposed technical solutions. Accordingly, in spite of considerable progress made in this field, a micro-mechanical description of the behavior of encapsulated modifier in asphalt mixture is still lacking. The present study aims to contribute to this important topic, by studying experimentally and numerically the mechanical performance of asphalt mixtures modified with encapsulated healing agents. Particular attention is given to establishing a computationally efficient and robust modelling tool for evaluation of the local stress state arising around the capsules at various stages of asphalt mixture service life.

In this study, the effect of the capsules with thiol-containing urethane polymer on the self-healing performance of a stone mastic asphalt (SMA) is evaluated. The mixtures with various contents of healing capsules are manufactured and the performance of the capsules during the mixture production and compaction is examined with X-Ray computed tomography (CT). The effect of capsules on the self-healing properties of asphalt mixtures is evaluated based on the repeated damage and recovery tests. In order to investigate computationally the mechanical behavior of the capsules in SMA, a micromechanical model of SMA is developed based on the finite element method (FEM). In this model the asphalt mixture is represented as a four-phase material consisting of elastic aggregates, elastic healing agent capsules and air voids embedded into viscoelastic matrix, representing bituminous mastic, i.e. a dense mixture of bitumen with aggregates smaller than

71 μm. Viscoelastic properties of the mastic and capsule strength are measured with the dynamic shear rheometer (DSR) and with uniaxial compressive tests respectively. The developed model is used to examine the stresses in the capsules at three different cases of macro-scale loads applied to the mixture. The obtained numerical results indicate that the proposed modelling approach can capture the stress state in the capsules in a computationally efficient manner. Computational predictions concerning the capsules breakage at different load cases are compared with the observations from the experiments and the feasibility of using the developed model for optimizing the properties of the capsules to ensure their timely activation is discussed.

2 Problem formulation and methodology

Self-healing asphalt mixtures may be considered as four-phase materials, consisting of air voids, aggregates, binder, and capsules with a healing agent. They are subjected to different types of loads during their production and service life. In particular, during compaction mixtures undergo profound compressive and shear plastic deformations, [22]. During service, the mixtures are subjected to compressive and tensile loads, with magnitude and orientation of the loading depending on the location in asphalt layer, [23]. The response of the mixture is predominantly viscoelastic at this stage. Furthermore, initiation of cracks will give rise to local stress and strain concentrations in the asphalt mixtures. For effectively activating the encapsulated modifier it is crucial that the strength of the capsules allows them to survive mixture compaction. At the same time, the capsules should be sufficiently brittle and weak to break at excessive stresses arising due to crack formation in their vicinity, [14].

The healing capsules may be approximately considered as spherical shells, with wall thickness, h, and diameter, D, containing the healing agent, as illustrated in Fig. 1a. It has to be pointed out, that this representation of capsule's geometry is a simplification—as reported in [11] in reality the capsules are sponge-like structures containing several pockets of healing agent. The implications of this simplified description of the capsule's geometry for the numerical analysis are discussed in somewhat more detail in Sect. 4 below. The thickness and/or diameter of the

capsules may be controlled by adjusting their production process such that capsules with different strength characteristics may be obtained. An increase in the thickness of the capsules' walls and decrease of their diameter increases the strength of the capsules, as discussed in detail in [24]. This dependency is also shown in Fig. 1b where, following the results presented in [24], for the capsules where calcium alginate shell is used for encapsulation, the diameter, strength and wall thickness of the capsules are shown as a function of ratio of rejuvenator agent (RA) to alginate (A). The capsules geometrical design and mechanical properties may thus be adjusted in order to ensure their optimal performance provided that the stress state induced in capsules at various load cases is known.

In this study the mechanical behavior of SMA mixtures containing capsules with the healing agent is investigated experimentally and numerically at constant temperature. The capsules content in the mixture evaluated ranges from 0 to 13.5% by weight. Micromechanical modelling is employed in order to investigate the stress state in the capsules under three macro-scale loading cases: tri-axial compression, uniaxial tension and uniaxial tension in presence of a notch for crack simulation. The three evaluated loading cases are intended to represent mixture compaction, service condition and damage initiation respectively. The viscoelastic properties of the SMA mastic phase and strength of the capsules are measured with the DSR and uniaxial compressive test respectively. The performance of the healing capsules during mixture production and their effect on mixtures self-healing properties is examined experimentally based on X-Ray CT measurements and on uniaxial compressive strength tests. The numerical and experimental methods used in this study are summarized in Sects. 2.1 and 3 below.

2.1 Micromechanical model

A multiscale modelling approach is used, as presented by Fadil et al. [25], where a micromechanical model of asphalt mortar is utilized as an intermediate model to provide the homogenized viscoelastic mortar matrix properties for an asphalt mixture model. This approach was chosen for its computational efficiency. Therefore, the modelling approach uses two separate size scales, where aggregates sizes between 2.5 and 10.0 mm are assigned to asphalt mixture scale model

(a)

(b)
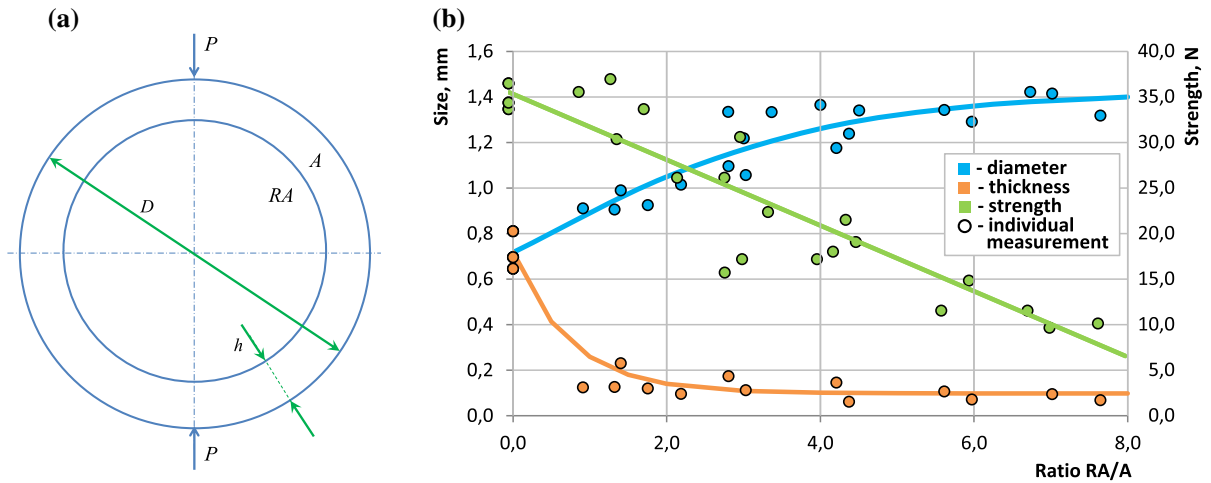
Fig. 1 **a** Geometry of capsules under uniaxial compression and **b** dependence of capsule geometry and strength on RA/A

together with the healing capsules and air voids, while the aggregates sizes between 0.16 and 2.5 mm are assigned to the mortar scale model as outlined in Fig. 2a.

In the mortar scale model the material is assumed to be composed of bitumen based mastic, as a matrix, and randomly distributed spherical aggregates. Periodic boundary conditions (PBCs) are employed to reduce

the size of the mortar modelled representative volume element (RVE), following the procedure developed in [26]. On the other hand, the micromechanical model for the asphalt mixture scale has been developed for a RVE of the asphalt mixture with capsules. The model contains 4 phases: an elastic aggregate phase, an elastic capsules phase, an air voids phase and a viscoelastic matrix representing asphalt mortar. The

Fig. 2 **a** The multiscale modelling approach, **b** aggregates, capsules and air voids randomly distributed within RVE space
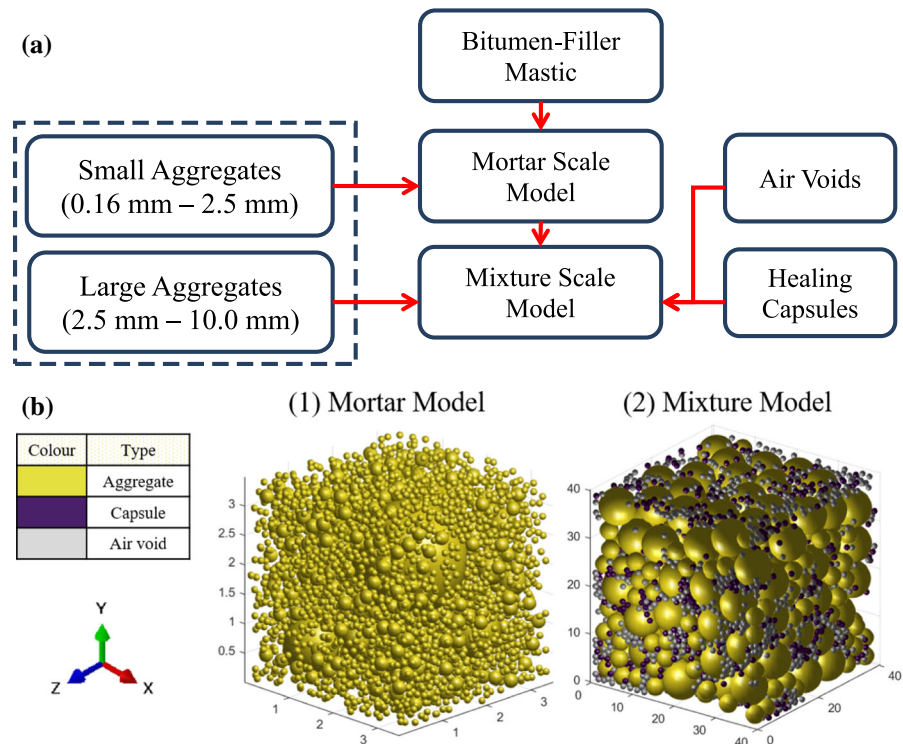
phases of the aggregates as well as the capsules are represented by randomly distributed elastic particles in the viscoelastic matrix, i.e. the mortar. Figure 2b shows the particles randomly distributed within the RVE space. The matrix is assumed to consist of isotropic linear viscoelastic material, with its properties described by two viscoelastic functions: the shear relaxation function, $G(t)$, and the viscoelastic Poisson's ratio, $v(t)$. Due to the experimental difficulties associated with measuring $v(t)$ [27], the bulk relaxation function, $K(t)$ is instead used to describe the binder. The generalized Maxwell model is used to describe $G(t)$ of the binder:

$$G(t) = G_o - \sum_{i=1}^{N} G_i \left[1 - e^{-t/\tau_i} \right] \tag{1}$$

where N is the number of elements in the Prony series, G_o is the instantaneous shear modulus or $G(t=0)$, while G_i and τ_i are the modulus and the relaxation time for the ith element of the Prony series respectively.

The mechanical viscoelastic properties of the mortar matrix, $G(t)$ and $v(t)$, are obtained as homogenized viscoelastic properties of the mortar scale micromechanical model. In the mortar scale model, the viscoelastic matrix represents the mastic phase and its properties are measured by a dynamic shear rheometer (DSR) frequency sweep test. These DSR measurements are converted to the time domain using the Schapery and Park approximate interconversion method [28].

In order to identify the homogenized viscoelastic properties of the mortar, the RVE of the mortar model is loaded uniaxially, with a constant tensile strain, $\overline{\epsilon}_x = 2\%$, at the start of the simulation as defined by Eq. (2):

$$\overline{\epsilon}_x(t) = 2\% \times H(t) \tag{2}$$

where $H(t)$ is the Heaviside step function. The homogenised time-dependent Poisson's ratio, $\overline{v}(t)$, as well as the relaxation function $\overline{E}(t)$ are then obtained from the volume average strains and stresses, $\overline{\epsilon}_y(t)$, $\overline{\epsilon}_z(t)$ and $\tilde{\sigma}_x(t)$ of the mortar scale model as follows:

$$\overline{v}(t) = -\frac{\overline{\epsilon}_y(t) + \overline{\epsilon}_z(t)}{2\overline{\epsilon}_x(t)} \tag{3}$$

$$\overline{E}(t) = \frac{\tilde{\sigma}_x(t)}{\overline{\epsilon}_x(t)} \tag{4}$$

Using the loading defined by Eq. (2), simplifies the analysis, as the elastic–viscoelastic correspondence principle is applicable in this case also on relations including the Poisson's ratio [27]. Therefore, Hooke's law can be used in the Laplace domain to obtain linear viscoelastic solutions.

The homogenised shear relaxation function, $\overline{G}(t)$, is calculated from $\overline{E}(t)$ and $\overline{v}(t)$ as in Eqs. (5) and (6); where Eq. (5) is obtained using the elastic–viscoelastic correspondence principle of the elastic relation shown in Eq. (7).

$$s \times \widetilde{G}(s) = \frac{s \times \widetilde{E}(s)}{2(1 + s \times \widetilde{v}(s))} \tag{5}$$

$$\overline{G}(t) = \mathcal{L}^{-1}\left\{ \widetilde{G}(s) \right\} \tag{6}$$

$$G = \frac{E}{2(1 + v)} \tag{7}$$

where $\mathcal{L}^{-1}$ represents the inverse Laplace transform, and $\widetilde{G}(s), \widetilde{E}(s)$ and $\widetilde{v}(s)$ represent the Laplace transforms to the s-domain of $\overline{G}(t)$, $\overline{E}(t)$ and $\overline{v}(t)$ respectively.

The mixture scale model is used to assess the stresses arising in the healing capsules at three different macro-scale load cases applied to SMA. Namely, the RVE was subjected to the following load cases, as is also illustrated in Fig. 3: (1) a triaxial compressive load of $\sigma = 1$ MPa, (2) a uniaxial tensile strain of $\epsilon_x = 0.03\%$ and (3) a notched model of the RVE under action of uniaxial tensile strain. In loading case (3), the simulated notch has length of 22.5 mm and width of 1 mm. The loading case (1) above is chosen in order to capture the stresses arising at healing capsules when mixtures are subjected to high levels of compressive stresses pertinent to compaction. Loading cases (2) and (3) are intended to represent the intact and damaged asphalt material at the bottom of SMA layer during the roads service life.

3 Experimental study

Mechanical behavior of self-healing SMA mixtures is examined experimentally. The materials and tests methods used in this study are summarized in Sects. 3.1 and 3.2 respectively.

(1) RVE – Compressive Load   **(2) RVE – Tesnile Load**   **(3) Notched RVE – Tesnile Load**
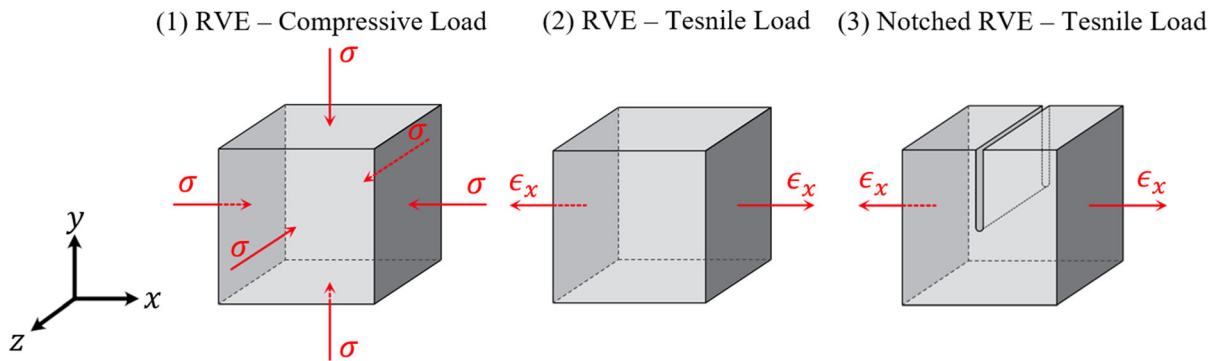
Fig. 3 Different loading cases used in the model

3.1 Materials

BND 60/90 bitumen (Russian state standard 22,245–90) with a softening point of 51°C (ASTM D36/D36M-20, EN 1427:2015) is used as a binder for asphalt concrete.

As self-healing promoting agent, an AR-polymer reducing agent was used. AR-polymer is a thiol-containing urethane polymer with terminal mercaptan groups (SH-), produced by «PolyMix Kazan» LLC following TU 2226–001-90,014,974–11. The hardener used for the polymer is tetramethyl thiuram disulfide $C_6H_{12}N_2S_4$. The mechanism of action of this healing agent consists in wetting the surface of the defect, partial diffusion into the matrix, polymerization, and "gluing" of the crack. As reported in previous studies by the authors, the AR polymer is found to be more effective in promoting asphalt mixture healing as compared to more traditional healing agents, such as sunflower oil, cf. [24].

In the present study, SMA mixtures with different contents of healing capsules 1.5, 3.0, 4.5, 9.0 and 13.5% by weight of bitumen (corresponding to 0.105, 0.21, 0.31%, 0.63 and 0.945% by weight of mixture) were prepared. The capsules were added at the stage of mixing dry components. The encapsulation of the reducing agent was carried out using alginate technology, by which calcium alginate capsules are formed. An aqueous solution based on sodium alginate ($C_6H_7O_6Na$), which is a sodium salt of alginic acid extracted from brown algae, is used for encapsulation [31]. The technological process for encapsulating a treating agent includes five main stages: preparation of an alginate solution using a high-speed stirrer, preparing an alginate emulsion of a healing agent using a

high-speed stirrer, dividing the alginate emulsion into separate drops, fixing individual drops of alginate emulsion through a solution of calcium salt and drying of alginate balls. The technological scheme of encapsulation of the healing agent is shown in Fig. 4a [9, 16, 19, 35].

The calcium salt solution is prepared in a forced-action mixer until $CaCl_2$ is completely dissolved in water. To prepare an alginate emulsion, sodium alginate is first added to water, which is mixed with a high-speed mixer (at least 2000 rpm), after which a healing agent is added to the resulting solution, from which an emulsion is formed. The resulting emulsion is divided into individual particles (alginate balls) using a separating funnel, which is fixed with calcium ions, passing through a bath with a solution of calcium salt. Alginate balls are dried to constant weight at a temperature of 50°C at the final stage. The appearance of the encapsulated healing agent is shown in Fig. 4b. The capsules had a diameter of 1.30 ± 0.05 mm with a wall thickness of 0.10 ± 0.005 mm. The healing content was (83 ± 2)%.

The SMA mixtures were prepared, based on the standard [29], with the aggregate gradation presented in Table 1. For all healing capsules contents, the binder content was set to 7%, resulting in an air void content of 3%, 2.9%, 2.9%, 2.8%, 2.6%, and 2.4% for the capsules contents of 0, 1.5, 3.0, 4.5, 9.0 and 13.5% correspondingly. 0.3% by weight of cellulose fibers Viatop-66 is used as a stabilizing additive to prevent segregation. Manganese oxide, sulfur, and tetramethyl thiuram disulfide (TMTD) were added to modify the binder when using the encapsulated AR-polymer in the composition of SMA. Modifiers were added to bitumen as hardeners and catalizators for the
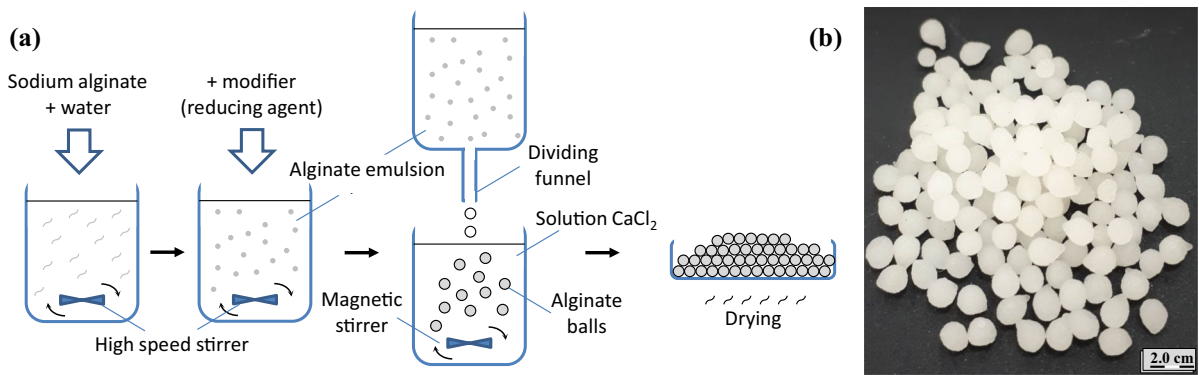
Fig. 4 a Encapsulating modifier (healing agent) schema, b encapsulated healing agent

Table 1 Sieve grain analysis (particle size distribution)

Parameter	Value							
Sieve size, mm	10	5	2.5	1.25	0.63	0.315	0.16	0.071
Passing, %	100	37.3	27.2	21.8	18.7	18.3	15.8	12.6

polymerization process of the released AR-polymer. Namely, to prepare a complex binder, 0.33% TMTD, 1.22% manganese oxide, and 2.00% sulfur by weight of bitumen were added to the bitumen heated to a temperature of 120°C.

SMA cylindrical specimens with a height and diameter of 71.4 mm were manufactured, following the standard [30], by placing the required mass of the mixture into a mold (inner height and diameter are 160 and 71.4 mm) and compacting it in two stages. First vibration compaction has been applied for 3 min followed by hydraulic press compaction.

3.2 Mechanical characterization

In order to obtain the input parameters for the micromechanical model described in Sect. 2.1, the strength of the capsules with the healing agent and complex modulus of mastic phase were measured. The strength of capsules was measured at room temperature in uniaxial compression test. The ultimate load was determined with a mechanical Uniframe press using a dynamometer with a maximum measuring limit of 1 kN. In the test, the capsules were placed between two rigid plates and compressed in load controlled mode, the compressive strength of the

capsules was determined as the maximum load registered during the test.

The load application rate during the test was maintained at a constant level of 10 N/s. The maximum compressive load for capsules with different wall thicknesses, h, and diameters, D, has been measured. For each h, D combination three measurements have been performed and the average measured failure loads, P, are reported in Table 2 along with the observed scatter, ΔP. As may be seen in Table 2, increasing the ratio of healing agent to alginate, RA/A, increases the ratio between wall thickness and diameter, of the capsules which in turn results in profound increase in maximum compressive load sustained by capsules.

Viscoelastic properties of the mastic were determined at 10°C, 20°C, and 30°C using the Dynamic Shear Rheometer Kinexus DSR using a frequency sweep tests in the frequency range of $\omega = 0.1\ldots10$ Hz at a shear strain of 0.1%. The mastic specimens were prepared by mixing 60% by weight of filler with the binder using an overhead mixer IKA RW 20 Digital. The test was carried out by EN 14,770–2006.

The internal structures of the SMA specimens with an encapsulated healing agent were studied by X-Ray CT using a VTOMEX M300 tomograph, General Electric. Scanning of the sample was carried out

Table 2 Properties of the capsules with different RA/A ratio

Parameter	Parameter value								
RA/A	0	1	2	3	4	5	6	7	8
h, mm	0.717	0.258	0.140	0.109	0.101	0.099	0.098	0.098	0.098
D, mm	0.72	0.89	1.05	1.17	1.26	1.30	1.36	1.38	1.40
h/D	1.00	0.29	0.133	0.093	0.080	0.076	0.072	0.071	0.070
P, N	35.5	31.9	28.3	24.7	21.0	18.0	13.8	10.2	6.6
ΔP, N	± 0.90	± 0.89	± 0.77	± 0.68	± 0.58	± 0.50	± 0.37	± 0.29	± 0.18

"layer by layer" with the further transformation of 2400 cross-section images into a 3-D model. Scan mode parameters were as follows: the voxel size used was 39.909 μm, the X-ray voltage and current were 270 kV and 180 μA respectively. The X-Ray beam was pre-hardened with the 1.0 mm Cu + 0.5 mm Sn filter.

The effect of capsules on the self-healing properties of asphalt mixtures is evaluated based on the compressive strength tests. The compressive strength tests were conducted at a temperature of 20°C and at 3 mm/min load rate. In order to calculate the healing index (HI) the tests were performed in cyclic fracture and recovery mode. Each cycle consisted of a compressive strength test followed by 7 days of healing at 20°C. For each content of healing capsules, the SMA mixtures were tested with 4 fracture and recovery cycles, i.e. the test program included 4 compression tests and 3 healing periods. A substantial amount of damage is introduced in the tests, with mixtures exhibiting certain amount of dilation, in particular after the 3rd and 4th test. It is accordingly expected that only part of the induced cracks would be recovered fully during healing periods.

4 Computational study

A micromechanical model for the SMA mixture containing healing capsules has been developed following the procedure described in Sect. 2.1. The numerical study is focused on the case of SMA mixture with a capsules content of 1.6% by volume, which approximately corresponds to the case of capsules content of 9.0% by weight of the binder. The mortar and the asphalt mixture models utilized cubic RVEs, with dimensions of $L \times L \times L$, with $L =$ 3.74 mm for the mortar model and $L = 40$ mm for the asphalt mixture. The aggregates, capsules as well as the air voids are idealized as spheres, as shown in Fig. 2b. These spheres are randomly distributed within the RVE while the viscoelastic matrix fills the remaining cubic volume. The sizes of spheres used were set to the average size of the spheres within each sieve. As Table 3 shows, the sizes of the spheres were picked based on the aggregates' sizes distribution reported in Table 1.

The number of spheres was calculated based on the chosen RVE size, the sphere size and volumetric proportions of aggregates as a percentage of the total volume of aggregates. The proportions for the RVEs, are calculated to follow the volumetric composition of SMA described in Sect. 3. The spheres representing the air voids were chosen to be equal to the capsule diameter, $d = 1.3$ mm, to avoid generating a large number of spheres and to reduce the computational time. Hence, 2122 spheres for air voids and 1132 spheres for healing capsules were used in the model.

The models are generated in LAMMPS according to the methodology detailed in Fadil et al. [25, 26]. The elements for meshing were tetrahedral quadratic elements. The models for the mortar and mixtures consisted of 500,00 to 800,00 elements.

The aggregates were assumed to be linear elastic, with Young's modulus, E = 39.3 GPa and Poisson's ratio ν = 0.23, corresponding to elastic parameters of limestone [32]. Young's modulus for the capsules was assumed to be $E_c = 3$ GPa.

The complex shear modulus for matrix in the mortar model is assumed to have viscoelastic properties corresponding to measured mastic properties. The complex bulk modulus, $K^*(\omega)$, was assumed to be constant and equal to $K^*(\omega) = 2336$ MPa as measured by [33] at 20 °C. The DSR measurements have been

Table 3 The number of spheres representing aggregates in the RVE and the volumetric proportions of the components of each RVE as a percentage of the total RVE volume

		Mixture model		Mortar model				
Aggregates	Sphere diameter (mm)	7.5	3.75	1.875	0.94	0.473	0.238	0.1155
	No. of spheres	146	189	1	7	7	335	3757
	Volume proportion (%)	50.64	8.16	11.95	6.85	0.90	5.52	7.07
Matrix	Volume proportion (%)	36.6		67.7				
Capsules		1.6		–				
Air voids		3.0		–				

converted into relaxation moduli $G(t)$ using the Schapery and Park approximate interconversion method [28]; the $G(t)$ is then fitted with Prony series, Eq. (1), with $n = 13$. The viscoelastic properties of the mortar, $G(t), v(t)$, are obtained by using the mortar micromechanical model as explained in Sect. 2.1.

In order to determine the maximum tensile and compressive stresses induced in capsules in the uniaxial compressive tests, a simple axisymmetric FE model for the test is used. It should be reminded that capsules are modelled as elastic balls, similarly to the SMA mixture model. This representation of capsules' geometry does not fully capture the reality, as the capsules shells contain several pockets of healing agent more or less randomly distributed throughout the capsule, cf. [11]. As the geometries of those individual pockets are not well defined, some approximation of the capsule's shape for numerical modelling is however necessary. The approximation used may result in a certain error in the determined tensile and compressive strengths of the capsules. The effect of those errors on the modelling predictions regarding the capsules breakage in SMA, is minimized by using the same geometry approximation in SMA modelling and individual capsule analysis.

In the model, the vertical compressive load, P, is transferred to the capsule through a rigid plate, the load is monotonically increased from 0 to 25 N. Hertzian contact interaction is defined between the plates and the capsule model. From the maximum compressive force values, reported in Table 2 the tensile and compressive strength of the capsules may thus be determined. As reported in Table 2, the capsules used in the present experimental study had the maximum forces in the range of P = 17.5…18.5 N. Accordingly their tensile and

compressive strengths, S_t and S_c, may be estimated to be in the range of $S_t = 12…13.5$ MPa and $S_c = 500…550$ MPa.

## 5 Results and discussion

First, the stress state induced in the capsules is examined numerically for the three load cases outlined in Sect. 2.1:

Load case 1: a tri-axial compressive load of $p = 1$ MPa;

Load case 2: a uniaxial tensile strain of $\varepsilon_x = 0.03\%$;

Load case 3: a notched model of the RVE under action of uniaxial tensile strain.

In Fig. 5a, b, the distribution of minimum principal strains in SMA is reported for the load case 1. The results in Fig. 5a, b are presented for the time under load $t = 1e - 4s$ and $t = 1e + 4s$, respectively. In order, to highlight the stress concentrations in the mortar phase the aggregates are removed in Fig. 5a, b. As may be seen in the figures, the relaxation in the matrix phase with time results in profound increase of compressive strains, with maximum compressive strains increasing by approximately a factor of 2.5, during the first 10e4 seconds under load. In Fig. 5c, d, the maximum principal stresses arising in healing capsules at load case 1 and $t = 1e - 4s, 1e + 4s$ is shown. It is seen that increase in compressive deformation, as presented in the figures, results in significant increase of local tensile stresses in the capsules. In particular, as seen in Fig. 5d at $t = 1e + 4s$, a considerable portion of capsules experiences tensile stresses above 1 MPa.
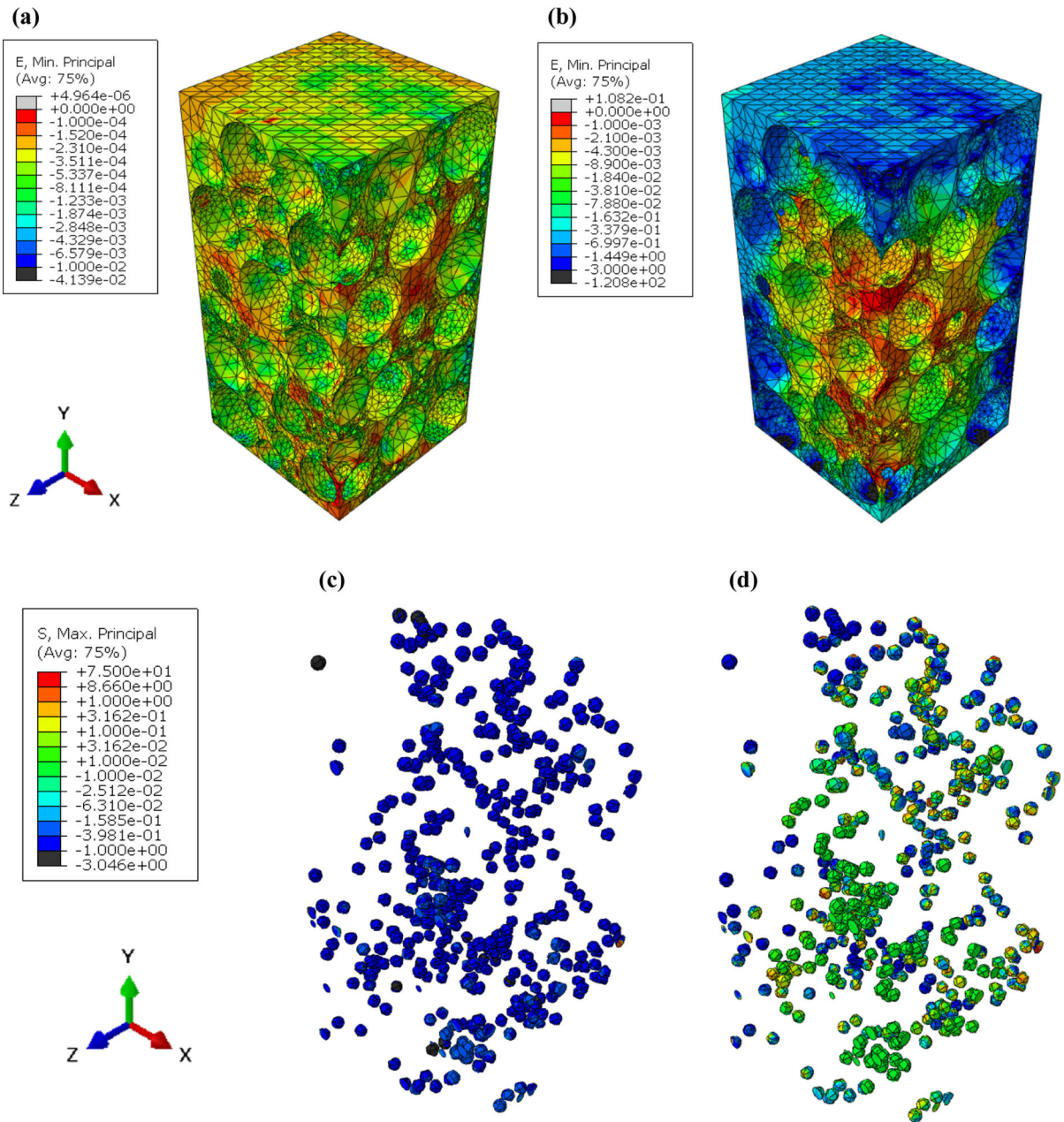
Fig. 5 SMA at tri-axial compression (load case 1) showing the distribution of minimum principal strains at **a** $t = 1e - 4s$; **b** $t = 1e + 4s$ as well as the distribution of maximum principal stresses in the healing capsules at **c** $t = 1e - 4s$; **d** $t = 1e + 4s$

As seen in Figs. 5c, d the stresses induced in the capsules vary in a wide interval depending on their location in the mixture. Accordingly, the capsules propensity to breakage is best evaluated from statistical point of view. In order to gain a better quantitative insight into stresses induced in the capsules at load case 1, cumulative probability distributions of

maximum and minimum principal stresses induced in capsules are presented in Fig. 6a, b. For a given stress level, σ_c, cumulative probability, $F_\sigma(\sigma_c)$, is calculated according to Eq. (8).

$$F_\sigma(\sigma_c) = \frac{n_{\sigma \leq \sigma_c}}{N_{total}} \cdot 100\% \tag{8}$$
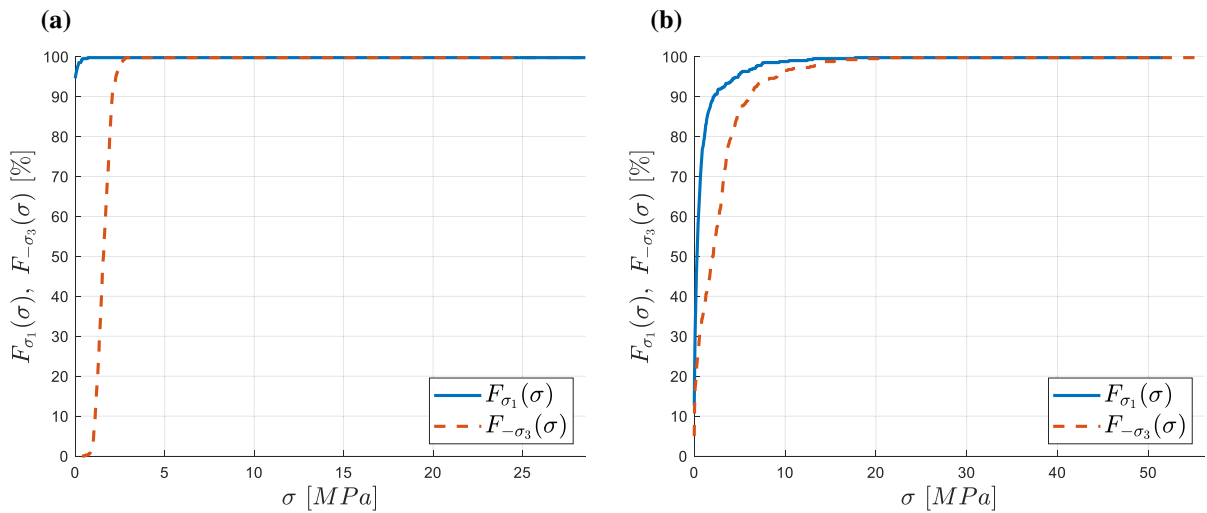
Fig. 6 Cumulative probability distributions of maximum (σ_1) and minimum ($-\sigma_3$) principal stresses experienced by capsules (load case 1); **a** $t = 1e - 4s$; **b** $t = 1e + 4s$

where $n_{\sigma \le \sigma_c}$ is a number of healing capsules subjected to stresses less than or equal to σ_c, and N_{total} is the total number of capsules in the volume. As seen from Eq. (8), $F_\sigma(\sigma_c)$ denotes a share of the capsules subjected to stresses below σ_c. For example, if for a given loading scenario $F_{\sigma=\sigma_1}(S_t)$=90%, where σ_1 is the maximum principal stress and S_t is the tensile strength of the capsules, 10% of the capsules may be expected to break.

As seen in Fig. 6a, at $t = 1e - 4s$, all the capsules in the mixture are subjected to stresses which are significantly smaller than their measured tensile and compressive strengths, S_t and S_c. In particular, the maximum tensile stress, σ_1, induced in the capsules is approximately 1.8 MPa; and for 90% of the capsules their maximum tensile stress is below 0.5 MPa. The maximum compressive stress, σ_3, induced in the capsules at $t = 1e - 4s$ is 5.5 MPa and below 2 MPa for 90% of capsules' volume. At the same time, the stresses induced in capsules grow as a function of time and at $t = 1e + 4s$ (Fig. 6b), 3% of the capsules are subjected to tensile stresses exceeding their tensile strength. It may thus be concluded that a small portion of the capsules may be expected to break when SMA is subjected to tri-axial compressive pressure of 1 MPa. The majority of capsules, are however still subjected to moderate stresses at $t = 1e + 4s$. For instance, as seen in Fig. 6b, 90% of the capsules are subjected to tensile stress below 2 MPa, which is significantly

smaller than their measured tensile strength, S_t, presented in Sect. 4.

In Fig. 7, the results analogous to the ones presented in Fig. 6 are presented for the case of SMA mixture loaded in uniaxial tension (i.e. load case 2). As tensile load is applied in strain controlled mode, the stresses in the capsules decrease with time under load. As observed in Fig. 7a the maximum compressive stresses induced in capsules are quite small, below 1.3. MPa, i.e. below 0.5% of the measured, compressive strength, S_c, of capsules. At the same time, the tensile stresses induced in capsules are much closer to their measured S_t, with maximum tensile stresses being approximately 7.2 MPa, and 10% of capsules subjected to tensile stresses above 3.8 MPa, which is approximately 60% and 30% of their S_t.

The maximum principal stress distribution for the load case 3, i.e. uniaxial tension in presence of notch, is shown in Fig. 8a. As expected, the presence of notch results in tensile stress concentration in front of the notch tip. As is also seen in Fig. 8a this stress concentration reaches approximately 24 MPa. These tensile stresses decrease fast with increasing distance from the notch tip and become nearly constant at 4 mm distance from it. The effect of these tensile stress concentrations on the stresses induced in healing capsules is examined in Fig. 8b, where cumulative probability distributions of maximum and minimum principal stresses induced in capsules at load case 3 are presented for $t = 1e - 4s$. As seen in Fig. 8b, the
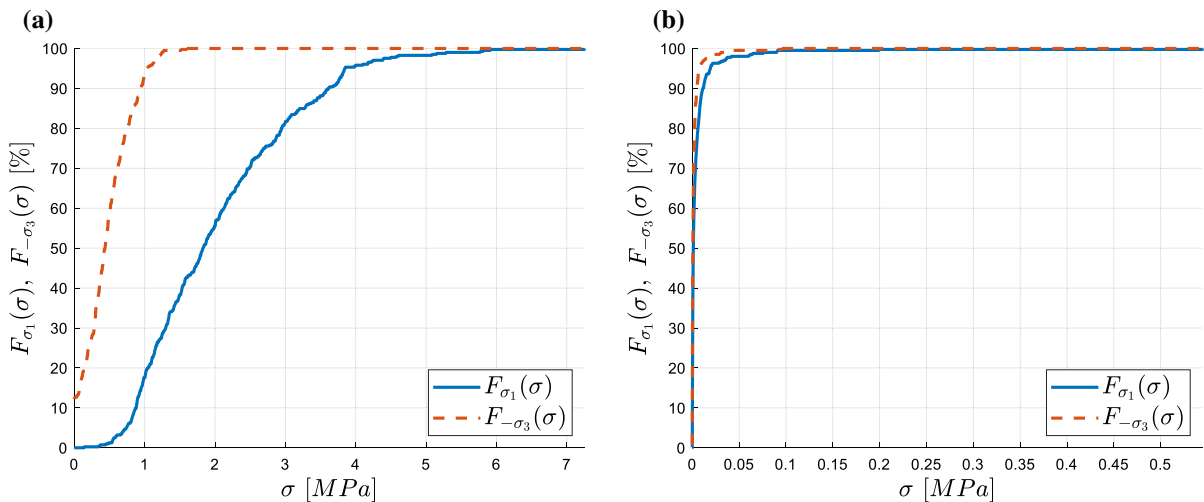
Fig. 7 Cumulative probability distributions of maximum (σ_1) and minimum $(-\sigma_3)$ principal stresses experienced by capsules (load case 2); **a** $t = 1e - 4s$; **b** $t = 1e + 4s$
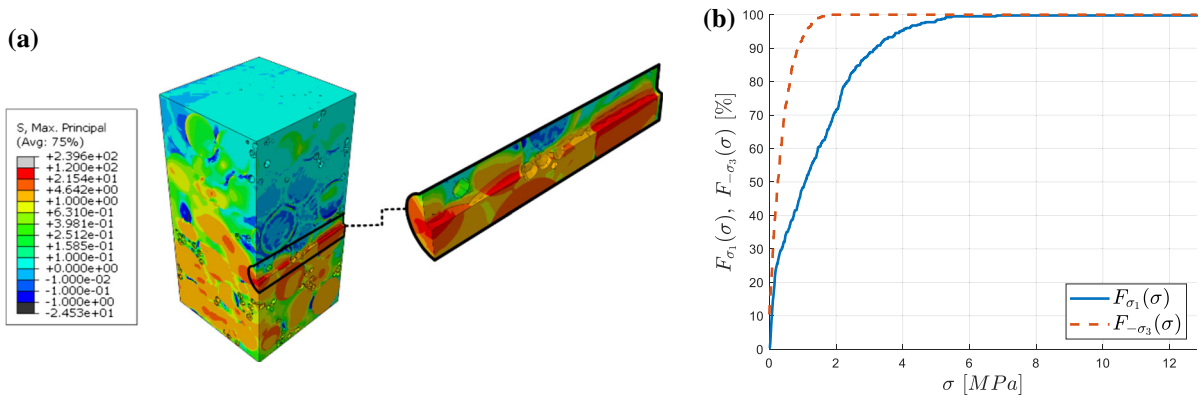
Fig. 8 a Distribution of maximum principal stress in notched SMA at uniaxial tension (load case 3), $t = 1e - 4s$; **b** cumulative probability distributions of maximum (σ_1) and minimum $(-\sigma_3)$ principal stresses experienced by capsules (load case 3), $t = 1e - 4s$

tensile stresses induced in the majority of the capsules do not change significantly due to presence of the notch. In particular, 90% of capsules experience tensile stresses below 3.8 MPa, which is very similar to observations in Fig. 7. At the same time, a small portion of the capsules, positioned in the vicinity of notch tip, experience significantly higher tensile stresses as compared to a notch free specimen. Namely, the maximum tensile stress in Fig. 8b is 12.5 MPa which is approximately 70% higher compared to the notch-free material.

The computational results presented in Figs. 5, 6, 7, 8, indicate that the proposed modelling approach allows to examine the stresses induced in healing capsules embedded in SMA at various macroscopic

load cases. It has to be pointed out, however, that the model developed in this study relies on simplified representation of SMA structure, with aggregates idealized as spheres. Accordingly, it may not fully capture the stress concentrations arising in capsules due to contact with real aggregate asperities. This realistic contact conditions may contribute to a significantly wider distribution of stresses in capsules as compared to the ones presented in Figs. 6, 7 and 8b. At the same time, the presented model allows to quantify the effect of change in SMA design and in loading conditions on the capsules stress state, in average sense. In particular, comparing the calculated maximum tensile and compressive stresses in capsules for the three load cases with the measured tensile and

compressive strengths of the capsules, S_t and S_c, of capsules the following expectations regarding their performance at various stages of SMA service may be formulated.

First of all, it appears that compressive stresses induced in capsules in all cases remain significantly below their S_c. Accordingly, with respect to capsules damage, their tensile loading is the most critical case. At tri-axial compaction (load case 1) some capsules experience tensile stresses close to their tensile strength, provided that the load is applied for sufficiently long time. Accordingly, some capsule breaking during compaction may be expected. The share of those capsules is, however, very small. The results presented in Fig. 7 furthermore indicate that, at uniaxial tension at strain level as approximately found at the bottom of asphalt layer, the stresses are sufficiently low to ensure that the capsules can survive without breaking. Examining the case of uniaxial tension in the presence of a notch (load case 3) shows that a small portion of capsules, located in the vicinity of the notch tip, experience much higher tensile stresses compared to the notch free situation. This increase of tensile stresses at load case 3 as compared to the load cases 1 and 2 allows to optimize the capsules design to ensure timely activation of the healing. For instance, based on the results presented in Figs. 6, 7 and 8b, it may be expected that capsules with $10 MPa \leq S_t \leq 12.5 MPa$ may survive mixture compaction (approximately 97% of the capsules) and traffic loads, but break with a crack tip in their immediate vicinity.

In order to validate the numerical results presented above, the samples of SMA with encapsulated healing agent were examined with X-Ray CT. The results of the CT images obtained on SMA specimen before strength testing are shown in Fig. 9. The specimen shown in Fig. 9 contains 3.0% of capsules by weight of the binder. In Fig. 9a, a 3D view of the specimen is presented with capsules indicated by red markers, in the figure the aggregate and binder phases were filtered out, in order to allow for capsules observation. It is seen that capsules are uniformly distributed throughout the mixture volume.

Through visual evaluation of CT images it was observed that absolute majority of capsules survived the mixture production. Approximately 5% of capsules were however damaged either during mixing or compaction processes. This finding is in at least qualitative agreement with computational results presented in Figs. 5 and 6. It should be pointed out that perfect quantitative agreement between modelling and experimental results may not be expected. In particular, as the mixing process is not evaluated in the model and as spherical aggregate shapes used in the model do not fully capture the stress concentrations arising in capsules due to their contacts with aggregates. Examples of capsules surviving the mixture production and broken during compaction are shown in Figs. 9b and c respectively.

The CT-scanning of SMA specimen has also been repeated after the first compressive strength test. In Figs. 10a, b a close-up CT images of the same capsule with healing agent obtained before and after strength test are shown. It may be seen in Fig. 10b that during the strength test a crack has formed in the vicinity of the capsule and as result the capsule was destroyed. Crack formed in the capsule is indicated with red pointer. The capsule thus sufficiently fulfilled its function by breaking when the crack formed at its vicinity. It has also been observed that after the strength test, the capsules located away from the cracks remained intact, accordingly maintaining their healing potential. The CT results in Figs. 9 and 10 indicate that the functionality of alginate containers is adequate, ensuring the survival of the capsules during hot mixture production and timely release of healing agent at damage initiation.

To determine the effect of capsules on self-healing properties of SMA, compressive strength of specimens containing various capsules content have been measured in cyclic fracture and recovery mode. Four cycles have been applied to each specimen, each cycle consisting of compressive strength test, where specimen was monotonically loaded in displacement control mode until the measured reaction force would start to decrease, followed by 7 days of recovery at 20°C.

The compressive strength measured at each cycle is reported in Table 4 for SMA mixtures healing capsules content of 0%, 1.5%, 3.0%, 4.5%, 9.0% and 13.5% by weight of the binder. As seen from the results presented in Table 4 for the cycle 1, addition of healing capsules reduces somewhat the initial strength of SMA. For instance, addition of 13.5% of capsules results in approximately 17% decrease of SMA strength. This may be explained by two factors. First of all, capsules and their interfaces with bitumen may
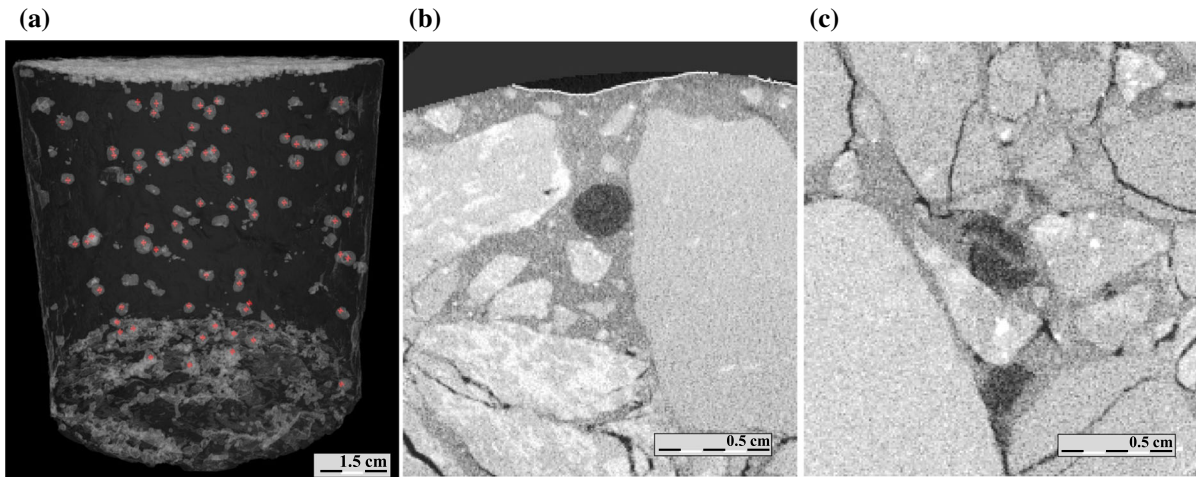
Fig. 9 CT images of SMA mixture after compaction **a** complete specimen view with capsules indicated by red markers; **b** a close up view of intact capsule; **c** a close up view of capsule damaged during compaction

Fig. 10 A close-up view of healing capsule embedded in SMA before **a** and after **b** strength test
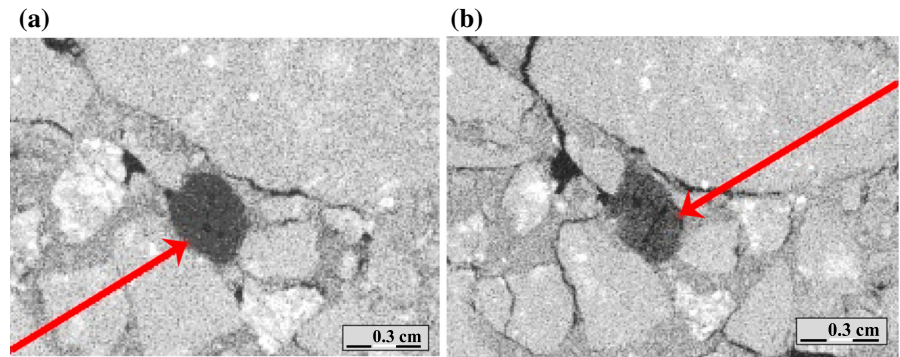
Table 4 Compressive strength of asphalt concrete with different content of healing capsules

Capsules content, %	Compressive strength at given cycle, MPa			
	1	2	3	4
0	4.02	3.40	3.03	2.91
1.5	3.70	3.33	2.99	2.92
3.0	3.59	3.25	3.17	3.06
4.5	3.55	3.20	3.06	2.91
9.0	3.42	2.86	2.60	2.38
13.5	3.35	2.81	2.57	2.27

act as stress concentrators in bituminous matrix promoting thus fracture initiation. Secondly, excessive capsules activation may result in more compliant response of SMA close to peak load.

At the same time, relative decrease in strength after 4 fracture and recovery cycles is smaller for SMA mixtures containing healing capsules as compared to SMA without capsules. In particular, the strength measured in the 4th cycle for the mixture without healing capsules is approximately 72% of the value measured in the 1st cycle. The corresponding number for the mixture containing 3% of the capsules is 85%, indicating better resistance to repeated loading. At the same time, the dependence is of SMA recovery

characteristics is non-linear as positive effects of capsules are offset by their negative influences in terms of stress concentrations and excessive softening of the binder phase. For instance, as seen in Table 4, the strength of SMA mixture with 13.5% of capsules measured in 4th cycle is 78% of the corresponding value measured for the mixture without capsules.

The effect of capsules content on the damage recovery in SMA is further explored quantitatively in Fig. 11, where healing index (HI) is presented as a function of test cycle and capsules content. HI is a measure commonly used to assess the healing, through the relative change of strength before and after healing [18, 19, 37–41]:

$$HI = \frac{R_h}{R_0} \cdot 100\%, \tag{9}$$

where HI is the healing index; R_h is strength after healing; R_0 is strength before healing.

As seen in Fig. 11, for all the capsules contents except 13.5%, the addition of capsules increases the HI of the mixtures, as compared to the reference mixture without the capsules. The most profound effect is observed in a case of SMA with 3% capsules content, where HI = 85% is observed after 4th testing cycle, this may be compared to 72% observed for the mixture without capsules. Accordingly it may be concluded that out of the contents of capsules examined, 3% is the optimal content for this SMA mixture, ensuring optimal healing characteristics without excessive negative effects. As may also be seen in Table 4, the SMA mixture containing 3% of healing capsules shows in 4th test cycle approximately 5% higher strength as compared to the mixture without healing capsules.
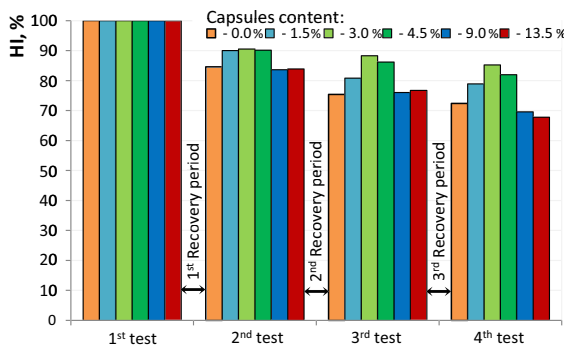
Fig. 11 HI of SMA after repeated compression tests with different contents of capsules

The experimental results presented in Figs. 9, 10, 11 and Table 4 indicate that the healing capsules successfully withstand the loads applied during mixture production and are broken only when damage forms in their vicinity. This findings are also in line with the computational observations discussed above. In particular, as seen from the modelling results presented in Figs. 6, 7, in absence of cracks at least 97% of capsules are subjected to stresses below their measured strength and accordingly are not expected to break. At the same time, as seen in Fig. 8, when crack forms in the material, the tensile stresses in the capsules located in the vicinity of the crack tip may exceed the capsule's strength resulting in its breakage and release of the healing agent.

6 Summary and conclusions

In this study, the mechanical behavior of the SMA mixtures containing capsules with the healing agent has been investigated experimentally and numerically. An FEM micromechanical model of asphalt mixture containing encapsulated binder modifier as healing agent is developed based on simplified computer-generated internal structures. The model is used to examine the stress state arising in capsules at different cases of macro-scale loads applied to the mixture. The macro-scale load cases evaluated in this study are assumed to be representative for loads experienced by the material during compaction, during service life and damage initiation. It is shown that the developed model can capture the stresses arising in healing capsules at different load scenarios. The numerical predictions concerning capsules breakage are at least in qualitative agreement with experimental findings. Accordingly, it appears to provide a feasible tool for optimization of capsules mechanical properties in order to improve their chance of survival during mixture production as well as their timely activation at damage initiation.

The effect of the capsules with thiol-containing urethane polymer (AR-polymer) on self-healing performance of a stone mastic asphalt (SMA) is also evaluated experimentally. Capsules were manufactured in the laboratory and it was possible to control their geometry and strength by varying the ratio of healing agent to the capsules wall made from alginate and AR-polymer as healing agent. The technological

process resulting in optimum capsules characteristics has been identified and SMA specimens with various volumetric contents of capsules have been manufactured. X-Ray computed tomography (CT) has been employed in order to investigate possible damage of capsules during mixture production. It is observed that the majority of capsules remain intact during compaction, which is also in line with the numerical observations.

The effect of healing capsules on damage recovery of SMA is examined experimentally based on repeated fracture recovery tests. It is shown that, for most capsules contents examined, capsules improve SMA healing characteristics. The magnitude of this improvement depends furthermore on the capsules content in a nonlinear fashion, as the beneficial effects of capsules are reduced by their negative influences in terms of stress concentrations and eventual excessive softening of the binder phase due to excessive activation of capsules. The fracture-recovery test results indicate that, for the mixture design used in the present study, optimal capsules content is 3% by weight of the binder. The loss of strength of SMA with 3% capsules content after four fracture-recovery tests was found to be 46% less as compared to the mixture without capsules. The effect of capsules on strength recovery may be potentially improved further provided that their size distribution and/or strength properties are optimized in order to ensure their gradual activation with the progression of fatigue damage. In this context, the micromechanical modeling approach proposed in this study may be particularly instrumental as it allows to identify the target capsule properties for different macro-scale load cases applied to the mixture. This direction will be explored as part of the future studies.

Availability of data and material Not applicable.

Code availability Not applicable.

Declarations

References

1. Partl MN (2018) Introduction. In: Partl, M.N., Porot L, Di Benedetto H, Canestrari F, Marsac P, Tebaldi G (eds), RILEM state-of-the-art report of RILEM TC 237-SIB, Testing and characterization of sustainable innovative bituminous materials and systems, vol. 24, pp. 1–14, Cham: Springer. 2018. Doi: https://doi.org/10.1007/978-3-319-71023-5_1

2. Leegwater G, Tabokovic A, Baglieri O, Hammoum F, Baaj H (2022) Terms and definitions on crack-healing and restoration of mechanical properties in bituminous materials. In: Proceedings of the RILEM international symposium on bituminous materials. ISBM 2020. RILEM Bookseries, vol 27, pp 47–53. Doi: https://doi.org/10.1007/978-3-030-46455-4_6

3. Su JF., Schlangen E, Qiu J (2013) Design and construction of microcapsules containing rejuvenator for asphalt. Powder Technol, vol 235, pp 563–571. Doi:https://doi.org/10.1016/j.powtec.2012.11.013

4. Al-Mansoori T, Norambuena-Contreras J, Garcia A (2018) Effect of capsule addition and healing temperature on the self-healing potential of asphalt mixtures. Mater Struct 51(2):1–12. https://doi.org/10.1617/s11527-018-1172-5

5. Su JF, Schlangen E (2012) Synthesis and physicochemical properties of novel high compact microcapsules containing rejuvenator applied in asphalt. Chem Eng J vol 198–199, pp. 289–300. Doi:https://doi.org/10.1016/j.cej.2012.05.094

6. Xue B, Wang H, Pei J, Li R, Zhang J, Fan Z (2007) Study on self-healing microcapsule containing rejuvenator for asphalt. Construct Build Mater 135:641–649. Doi:https://doi.org/10.1016/j.conbuildmat.2016.12.165

7. Al-Mansooria T, Micaeloabc R, Artamendid I, Norambuena-Contreras J, Garcia A (2017) Microcapsules for self-healing of asphalt mixture without compromising mechanical performance. Construct Build Mater 155:1091–1100. Doi: https://doi.org/10.1016/j.conbuildmat.2017.08.137

8. Inozemtcev S, Korolev E (2018) Surface modification of mineral filler using nanoparticles for asphalt application.

MATEC Web of Conf 196(10):04052. https://doi.org/10.1051/matecconf/201819604052

9. Inozemtcev SS, Korolev EV, Do TT (2021) Thermal and mechanical properties of Calcium alginate capsules for self-healing asphalt concrete. Mater Sci Forum 1041:101–106. Doi:https://doi.org/10.4028/www.scientific.net/MSF.1041.101

10. Anupam BR, Umesh CS, Chandrappa AK (2022) A methodological review on self-healing asphalt pavements. Construct Build Mater 321(08):126395. Doi:https://doi.org/10.1016/j.conbuildmat.2022.126395

11. Xua S, Tabaković A, Liua X, Schlangena E (2018) Calcium alginate capsules encapsulating rejuvenator as healing system for asphalt mastic. Construct Build Mater 169:379–387. Doi: https://doi.org/10.1016/j.conbuildmat.2018.01.046.

12. Bueno M, Kakar MR, Refaa Z, Wortlitschek J, Stamatiuo A, Partl MN (2019) Modification of asphalt mixtures for cold regions using microencapsulated phase change materials. Nat Res Sci Rep 9:10. https://doi.org/10.1038/s41598-019-56808-x

13. Alpizar-Reyes E, Concha JL, Martín-Martínez FJ, Norambuena-Contreras J (2022) Biobased spore microcapsules for asphalt self-healing. ACS Appl Mater Interfaces 14(27):31296–33131. https://doi.org/10.1021/acsami.2c07301

14. Wan P, Liu Q, Wu S, Zhao Z, Chen S, Zou Y, Rao W, Yu X (2021) A novel microwave induced oil release pattern of calcium alginate/ nano-Fe_3O_4 composite capsules for asphalt self-healing. J Clean Prod 297:126721. Doi: https://doi.org/10.1016/j.jclepro.2021.126721

15. Tabaković A., Faloon Ch. O'Prey D The effect of conductive alginate capsules encapsulating rejuvenator (HealRoad Capsules) on the healing properties of 10 mm stone mastic asphalt mix. App Sci 12(7):3648. Doi: https://doi.org/10.3390/app12073648.

16. Inozemtcev S.S., Korolev E.V. Technological features of production calcium-alginate microcapsules for self-healing asphalt. MATEC Web of Conferences. 2018. 251. 01008. DOI:https://doi.org/10.1051/matecconf/201825101008.

17. Xu S, Tabakovic A, Liu X, Palin D, Schlangen E (2019) Optimization of the calcium alginate capsules for self-healing asphalt. Appl Sci 9(3):468–480. https://doi.org/10.3390/app9030468

18. Al-Mansoori T, Norambuena-Contreras J, Micaelo R, Garcia A (2018) Self-healing of asphalt mastic by the action of polymeric capsules containing rejuvenators. Construct Build Mater 161:330–339. Doi:https://doi.org/10.1016/j.conbuildmat.2017.11.125.

19. Inozemtcev SS, Korolev EV (2020.) Review of road materials self-healing: problems and perspective. In: IOP conference series: materials science and engineering, vol. 855. p 012010. Doi:https://doi.org/10.1088/1757-899X/855/1/012010.

20. Xu Sh, García A, Su J, Liu Q, Tabaković A, Schlangen E (2018) Self-healing asphalt review: from idea to practice. Adv Mater Interface 5(17):1800536. https://doi.org/10.1002/admi.201800536

21. Sun D, Sun G, Zhu, Guarin A, Li B, Dai Z, Ling J (2018) A comprehensive review on self-healing of asphalt materials: Mechanism, model, characterization and enhancement. Adv Colloid Interface Sci 256:65–93. Doi: https://doi.org/10.1016/j.cis.2018.05.003.

22. Olsson E, Jelagin D, Partl MN (2019) New discrete element framework for modelling asphalt compaction. Road Mater Pavement Des 20(Sup2):S604–S616. https://doi.org/10.1080/14680629.2019.1633750

23. Zhang Y, Leng (2017) Quantification of bituminous mortar ageing and its application in ravelling evaluation of porous asphalt wearing courses. Mater Des 119:1–11. Doi: https://doi.org/10.1016/j.matdes.2017.01.052

24. Inozemtcev SS, Korolev EV (2021) Active polymeric reducing agent for self-healing asphalt concrete. In: IOP conference series: mMaterials science and engineering. 1030:012002. Doi:https://doi.org/10.1088/1757-899X/1030/1/012002.

25. Fadil H, Jelagin D, Partl MN (2022) Spherical indentation test for quasi-non-destructive characterisation of asphalt concrete. Mater Struct 55(3):1–16. https://doi.org/10.1617/s11527-022-01945-5

26. Fadil H, Jelagin D, Larsson PL, Partl MN (2019) Measurement of the viscoelastic properties of asphalt mortar and its components with indentation tests. Road Mater Pavement Des 20(sup2):S797–S811. https://doi.org/10.1080/14680629.2019.1628434

27. Hilton HH (2011) Clarifications of certain ambiguities and failings of Poisson's ratios in linear viscoelasticity. J Elast 104(1–2):303–318. https://doi.org/10.1007/s10659-010-9296-z

28. Schapery RA, Park SW (1999) Methods of interconversion between linear viscoelastic material functions. Part II—an approximate analytical method. Int J Solids Struct 36:1677–1699. Doi:https://doi.org/10.1016/S0020-7683(98)00060-2.

29. Russian state standard GOST 31015–2002 Bituminous stone mastic mixtures and stone mastic asphalt. Specifications, p 14. Link: https://internet-law.ru/gosts/gost/8440.

30. Russian state standard GOST 12801–98 Materials on the basis of organic binders for road and airfield construction. Test methods, p 63. Link: https://internet-law.ru/gosts/gost/43662.

31. Inozemtcev SS, Toan DT (2021) Sodium alginate application in self-healing technology for asphalt concrete. In: Klyuev SV, Klyuev AV (eds) Environmental and construction engineering: reality and the future. Lecture Notes in Civil Engineering vol 160, pp 59–65. Springer, Cham. DOI:https://doi.org/10.1007/978-3-030-75182-1_9.

32. Wang L (2011) Mechanics of asphalt: microstructure and micromechanics, 1st Edition. McGraw-Hill, New York. ISBN: 9780071498548. Retrieved from https://www.accessengineeringlibrary.com/content/book/9780071498548. Accessed 01 May 2022

33. Wolf K (2010) Laboratory measurements and reservoir monitoring of bitumen sand reservoir (Stanford University). Retrieved from https://pangea.stanford.edu/research/srb/docs/theses/SRB_122_JUL10_Wolf.pdf. Accessed 01 May 2022

34. Daintith JA (2009) Dictionary of Physics (6 ed.). Oxford University Press, Oxford

35. Inozemtcev SS, Korolev EV, Smirnov VA (2016) Nanomodified bitumen composites: Solvation shells and

rheology. Adv Mater Struct Mech Eng . Chap. 83, pp 393–397. Doi:https://doi.org/10.1201/b19693-84

36. Voyiadjis G, Bank LC, Jacobs LJ (2013) Mechanics of materials and structures. Elsevier Science B.V.

37. Qiu J, Wu S, Molenaar AAA (2009) Investigating the self healing capability of bituminous binders. Road Mater Pavement Des 10:81–94. Doi:https://doi.org/10.1080/14680629.2009.9690237.

38. Norambuena-Contreras J, Liu Q, Zhang L, Wu S, Yalcin E, Garcia A (2019) Influence of encapsulated sunflower oil on the mechanical and self-healing properties of dense-graded asphalt mixtures. Mater Struct 52(4):52–78. https://doi.org/10.1617/s11527-019-1376-3

39. Xu S, Tabaković A, Liu X, Palin D, Schlangen E (2019) Optimization of the calcium alginate capsules for self-healing asphalt. Appl Sci 9(3):468. https://doi.org/10.3390/app9030468

40. Tabaković A, Schuyffel L, Karač A, Schlangen E (2017) An evaluation of the efficiency of compartmented alginate fibres encapsulating a rejuvenator as an asphalt pavement healing system. Appl Sci 7(7):647. Doi:https://doi.org/10.3390/app7070647.

41. Shu B, Bao S, Wu S, Dong L, Li C, Yang X, Norambuena-Contreras J, Liu Q, Wang Q (2019) Synthesis and effect of encapsulating rejuvenator fiber on the performance of asphalt mixture. Materials 12(8):1266. https://doi.org/10.3390/ma12081266